Journal of Engineering Technology and Applied Physics

A Two-Equation Model for Forced Convection Heat Transfer in Porous Medium with The Effect of Heat Generation in the Solid

Jun Yang Lee[1, 3] and Gooi Mee Chen[2, 3, *]
[1]*School of Engineering, Monash University, Jalan Lagoon Selatan, Bandar Sunway, 46150, Selangor Darul Ehsan, Malaysia.*
[2]*Centre for Advanced Mechanical and Green Technology, CoE for Robotics & Sensing Technologies, Multimedia University, Jalan Ayer Keroh Lama, 75450 Bukit Beruang, Melaka, Malaysia.*
[3]*Faculty of Engineering and Technology, Multimedia University, Jalan Ayer Keroh Lama, 75450 Bukit Beruang, Melaka, Malaysia.*
[*]*Corresponding author*: gmchen@mmu.edu.my, *ORCiD*: 0000-0002-3046-715X
https://doi.org/10.33093/jetap.2026.8.1.13
Manuscript Received: 28 July 2025, Revised: 7 August 2025, Accepted:26 October 2025, Published: 15 March 2026

***Abstract*—This study analyses forced convection through a rectangular porous channel subject to uniform wall heat flux with internal heat generation in the solid phase, adopting a local thermal non-equilibrium model. Applying the Brinkman-extended Darcy velocity model, the forced convection problem is solved analytically, in terms of four key parameters, heat source ratio Q, fluid to solid effective thermal conductivity ratio κ, equivalent Biot number Bi and porous medium shape factor α . The exact solution is compared with one using Darcy velocity model. When the boundary effect is not taken into consideration in porous medium with low permeability, the heat transfer coefficient is overpredicted. Wall effects have also resulted in a higher critical value for the Q for the occurrence of dissimilarity in the sign of the fluid and solid wall temperature gradient.**

***Keywords*—Forced convection, Porous medium, Local Thermal Non-Equilibrium (LTNE), Thermally fully developed, Heat generation.**

I. INTRODUCTION

A porous medium consists of a solid matrix interspersed with void spaces, commonly known as pores. These pores can occupy a small to significant fraction of the total volume of the medium. Over the past few decades, porous media have gained increasing attention for their ability to enhance heat transfer. They have been widely employed across various industries [1], including electronics cooling [2, 3], geothermal energy systems, the petroleum sector, and nuclear reactor technology.

On the modelling of heat transfer in porous medium, detailed formulation can be found in Kaviany's work [4]. In general, two primary models are utilized to model energy equation in porous medium. One -equation model is based on the local thermal equilibrium (LTE) assumption, whereas two-equation model that accounts for the local thermal non-equilibrium condition (LTNE) needs to be considered when the temperature difference between the solid and fluid phase becomes significant [5], such as problems that involve internal solid heat generation. Marafie and Vafai [6] investigated forced convection flow through a channel filled with porous medium and constructed error maps for the validity of one-equation model for various physical conditions. On the other hand, Alazmi and Vafai [7] analysed various boundary condition for an isoflux thermal boundary problem found in the literature [8-11] under LTNE assumption. In their study, qualitative and quantitative interpretations of the results are utilized to investigate the prominent characteristics of the models under consideration.

The earliest phenomenological velocity model in porous medium is the Darcy velocity model, which is widely employed due to its simplicity [12]. Despite its

This work is licensed under the Creative Commons BY-NC-ND 4.0 International License.
© Universiti Telekom Sdn Bhd.
Published by MMU PRESS. URL: https://journals.mmupress.com/index.php/jetap/index

simplicity, Darcy velocity model fails to govern various flow conditions. It is unable to determine velocity profiles accurately near the impermeable surface that bounds the porous medium. As pointed out in the classical paper of Vafai and Tien [13], although the boundary effect results in very thin momentum boundary layer which is insignificant in overall flow consideration, its effect on heat transfer is pronounced when the thickness of thermal boundary layer is less than or of the same order as the momentum boundary layer. In addition to that, Poulikakos and Renken [14] showed that the effect of wall channelling is more significant when boundary effect is not taken into account, thereby leading to the overprediction of heat transfer. Other conditions in which Darcy law fails include fluid flow in high inertial flow regime [15] as well as developing flow [16]. In order to account for the effects aforementioned, Darcy velocity model is extended and the resulting velocity model is referred to as Brinkman-Forchheimer-extended Darcy momentum equation [17]. Hooman [18] investigated fully developed forced convection between parallel plates filled with porous media by applying the Brinkman–Forchheimer momentum equation. The problem was solved both numerically and asymptotically, with limiting-case results showing good agreement with existing numerical and analytical solutions in the literature.

In contrast, Lee and Vafai [1] employed a two-equation energy or LTNE model and the Darcy velocity formulation to study forced convection in a porous channel. Their work revealed that heat transfer mechanisms in porous media could be categorized into three regimes: fluid conduction-dominated, solid conduction-dominated, and interfacial heat transfer-dominated. They also developed a practical criterion to assess the validity of the one-equation model for channels with varying cross-sectional geometries.

Numerous works on forced convective heat transfer in porous medium have been undertaken. Nakayama *et al.* [12] analysed force convection in a porous channel by using one-equation model and Brinkman-extended Darcy velocity model. Exact and approximate solutions for the problem were developed, and excellent agreement was achieved between both solutions. Hooman [18] studied fully developed forced convection through a porous medium bounded by parallel plates by applying Brinkman-Forchheimer momentum equation. The problem is solved numerically as well as asymptotically, and the results of the limiting cases are found to be in good agreement with those available in the literature and numerical results. On the other hand, Lee and Vafai [1] solved forced convection in a porous channel using two-equation model and Darcy velocity. The study showed that heat transfer characteristics in porous medium can be classified into three regimes based on heat transfer mechanisms, namely fluid conduction, solid conduction and interfacial heat transfer between solid and fluid. The study also investigated and developed a practical criterion for the validity of one equation model applied to channels with different cross sections. Kim and Kim [19] modelled a microchannel heat sink as a fluid-saturated porous medium and derived analytical solutions for both velocity and temperature profiles using the Brinkman-extended Darcy momentum equation and a two-equation energy model. Their study identified key engineering parameters and analyzed their impact on heat transfer performance.

Yang and Vafai [20] examined the effects of internal heat generation on temperature profiles within a porous medium. Using a two-equation LTNE model and the Darcy momentum equation, they demonstrated the occurrence of opposite fluid and solid temperature gradients at the wall when internal heat generation in either phase becomes sufficiently large. Subsequently, Yang *et al.* [21] solved a fully developed forced convection problem in a porous tube under constant wall heat flux and LTNE conditions. Using aluminium foam and air as a representative case, they showed that significant temperature differences between fluid and solid phases persist in the core region, suggesting that the local thermal equilibrium (LTE) assumption may not hold when the solid-to-fluid thermal conductivity ratio is high.

Previous studies have examined Couette–Poiseuille flow in porous channels under fully developed conditions with unequal wall heat flux, emphasizing the role of internal heat generation in the form of viscous dissipation on heat transfer [22]. The Nusselt number and temperature field were found to depend on the Brinkman number, Reynolds number, and porous medium shape factor, where an increased permeability enhances convection near the moving wall. In microchannels, viscous dissipation intensifies at higher Reynolds numbers, leading to elevated peak temperatures. Under LTNE conditions, temperature variations were more pronounced due to shear effects, and deviations from LTE predictions became significant [23]. These findings highlight the critical influence of channel scale and porous structure on heat transfer behaviour Another study examines Couette–Poiseuille flow in a porous medium with asymmetric heat fluxes, showing that viscous dissipation, Brinkman number, and wall velocity significantly affect heat transfer [24]. LTE is achieved when interphase heat transfer is strong, highlighting the importance of LTNE when the interfacial heat transfer is not significant. The afore-mentioned studies however have not looked into the effects of internal heat generation in the solid phase analytically with an LTNE model.

In this study, the effects of internal heat generation within the solid phase on forced convection in a rectangular channel saturated with a porous medium are investigated. Internal heat generation in the solid phase is important in exothermic processes such as chemical reactions, radiation decay, and so on. The analysis is conducted using a two-equation energy model coupled with the Brinkman-extended Darcy momentum equation. Since the Brinkman-extended model incorporates the influence of wall friction and

boundary effects, particular attention is given to examining how the presence of the wall impacts the temperature profiles in both the fluid and solid phases with internal heat generations in solid.

II. PROBLEM FORMULATION AND ANALYTICAL RESULTS

The schematic diagram of the problem is illustrated in Fig. 1. A steady, unidirectional fluid flow is considered along the axial direction of the rectangular channel. The following assumptions are adopted in this study:

- The thermophysical properties of both the porous medium and the fluid are isotropic and constant.
- The fluid is incompressible.
- Viscous dissipation is negligible.
- Inertial effects are negligible.
- The flow is thermally and hydrodynamically fully developed.
- The solid substrates bounding the porous medium are impermeable, possess finite thickness, and have high thermal conductivity.

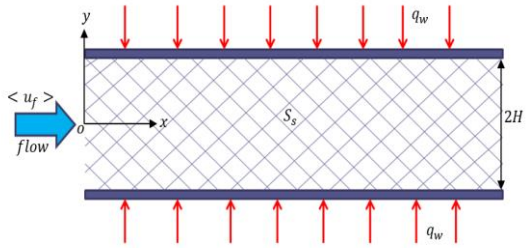

Fig. 1. Schematic diagram of the problem.

A. Velocity Profile

To account for wall effects, the Brinkman-extended Darcy momentum equation is solved in conjunction with the appropriate boundary conditions [25];

$$u = Da\left(1 - \frac{\cosh(\alpha\eta)}{\cosh(\alpha)}\right) \tag{1}$$

, where α is the porous medium shape factor and is given as:

$$\alpha = \sqrt{\frac{1}{MDa}} \tag{2}$$

B. Temperature Profile

The LTNE assumption is employed in this study, and the corresponding two-equation energy model is expressed as follows [11, 26]:

Fluid:

$$\rho_f c_{pf} < u_f > \frac{\partial < T >^f}{\partial x} = k_{f,eff}\frac{\partial^2 < T >^f}{\partial y^2} + h_{fs}a_{fs}(< T >^s - < T >^f) \tag{3}$$

Solid:

$$k_{s,eff}\frac{\partial^2 < T >^s}{\partial y^2} - h_{fs}a_{fs}(< T >^s - < T >^f) + (1-\varepsilon)S_s = 0 \tag{4}$$

The boundary conditions for the energy equations at the channel centreline and walls are defined as follows:

At $y = 0$:

Fluid:

$$\frac{\partial < T >^f}{\partial y} = 0 \tag{5a}$$

Solid:

$$\frac{\partial < T >^s}{\partial y} = 0 \tag{5b}$$

At $y = H$:

Fluid:

$$< T >^f = T_w \tag{6a}$$

Solid:

$$< T >^s = T_w \tag{6b}$$

Wall heat flux:

$$q_w = k_{f,eff}\frac{\partial < T >^f}{\partial y}\bigg|_{y=H} + k_{s,eff}\frac{\partial < T >^s}{\partial y}\bigg|_{y=H} \tag{7}$$

It is important to note that $(\partial\langle T\rangle f/\partial x)$ remains constant for a thermally fully developed flow subjected to a uniform wall heat flux [27]. By averaging the sum of the solid and fluid energy equations over the channel's cross-sectional area and incorporating Eq. (7), the following relationship is obtained:

$$\rho_f c_{pf}\frac{\partial < T >^f}{\partial x} = \frac{1}{< u_f >_m}\left(\frac{q_w}{H} + (1-\varepsilon)S_s\right) \tag{8}$$

It is noted that $\langle u_f\rangle_m$ represents the cross-sectionally averaged fluid velocity and can be determined using the following expression:

$$< u_f >_m = \frac{1}{2H}\int_{-H}^{H} < u_f > dy \tag{9}$$

Substituting Eq. (8) into Eq. (3) results in:

$$k_{f,eff}\frac{\partial^2 < T >^f}{\partial y^2} + h_{fs}a_{fs}(< T >^s - < T >^f) = \frac{< u_f >}{< u_f >_m}\left[\frac{q_w}{H} + (1-\varepsilon)S_s\right] \tag{10}$$

The governing energy equations are subsequently non-dimensionalized by introducing the following dimensionless temperature:

$$\theta_i = \frac{k_{s,eff}(< T >^i - T_w)}{q_w H}, i \in \{s, f\} \tag{11}$$

Together with the dimensionless length $\eta = y/H$, the energy equations can be expressed in the following non-dimensional form:

Fluid:

$$\kappa\theta_f'' + Bi\left(\theta_s - \theta_f\right) = \hat{u}(1+Q) \tag{12}$$

Solid:

$$\theta_s'' - Bi\left(\theta_s - \theta_f\right) = -Q \tag{13}$$

where κ, Bi, Q and $\hat{u}$ are respectively defined as:

$$\kappa = \frac{k_{f,eff}}{k_{s,eff}}, Bi = \frac{h_{fs}a_{fs}H^2}{k_{s,eff}}, Q = \frac{(1-\varepsilon)S_sH}{q_w}$$
$$\hat{u} = \frac{\alpha}{\alpha - \tanh\alpha}\left(1 - \frac{\cosh(\alpha\eta)}{\cosh(\alpha)}\right) \tag{14}$$

The dimensionless boundary conditions are given as:

At $\eta = 0$:

$$\theta_f' = 0 \tag{15a}$$
$$\theta_s' = 0 \tag{15b}$$

At $\eta = 1$:

$$\theta_f = 0 \tag{16a}$$
$$\theta_s = 0 \tag{16b}$$

After appropriate mathematical manipulation, the decoupled fluid-phase energy equation is obtained as:

$$\theta_f'''' - Bi(1+\kappa)\theta_f'' = BiQ + \frac{(1+Q)\alpha}{\alpha - \tanh\alpha}\left[\frac{\cosh(\alpha\eta)}{\cosh(\alpha)}(Bi - \alpha^2) - Bi\right] \tag{17}$$

The two additional boundary conditions required to solve Eq. (17) are given as:

At $\eta = 0$:

$$\theta_f''' = 0 \tag{18}$$

At $\eta = 1$:

$$\theta_f'' = 0 \tag{19}$$

The exact solutions for the dimensionless temperature profiles of the fluid and solid phases are given by:

$$\theta_f = A_1 + A_2\eta^2 + 2A_3\cosh(\gamma\eta) + A_4\cosh(\alpha\eta) \tag{20a}$$

$$\theta_s = A_1 + A_2\left(\eta^2 - \frac{2\kappa}{Bi}\right) + \left(1 - \frac{\gamma^2\kappa}{Bi}\right) 2A_3\cosh(\gamma\eta) + \left(1 - \frac{\alpha^2\kappa}{Bi}\right)A_4\cosh(\alpha\eta) + \frac{1+Q}{Bi}\hat{u} \tag{20b}$$

, where γ, A_1, A_2, A_3 and A_4 are given as:

$$\gamma = \sqrt{\frac{Bi(1+\kappa)}{\kappa}} \tag{21}$$

$$A_1 = -A_2 - 2A_3\cosh(\gamma) - A_4\cosh(\alpha) \tag{22}$$

$$A_2 = \frac{1}{2(1+\kappa)}\left(\frac{(1+Q)\alpha}{\alpha - \tanh(\alpha)} - Q\right) \tag{23}$$

$$A_3 = -\frac{2A_2 + A_4\alpha^2\cosh(\alpha)}{2\gamma^2\cosh(\gamma)} \tag{24}$$

$$A_4 = \frac{(1+Q)(Bi - \alpha^2)}{\alpha[Bi(1+\kappa) - \kappa\alpha^2]} \times 1/(\sinh(\alpha) - \alpha\cosh(\alpha)) \tag{25}$$

The Nusselt number, as defined in Eq. (26) [1], can subsequently be determined from the temperature profile.

$$Nu_w = \frac{h_wD}{k_{f,eff}} \tag{26}$$

Hence, the Nusselt number in dimensionless form is expressed as:

$$Nu_w = -\frac{4}{\kappa\theta_{fm}} \tag{27}$$

, where θ_{fm} denotes the dimensionless bulk mean fluid temperature, defined as:

$$\theta_{fm} = \frac{6}{(6\gamma\alpha^5 - 6\gamma^3\alpha^3)\cosh(\alpha)\left(1 - \frac{\tanh(\alpha)}{\alpha}\right)\{-\alpha^4A_3(\alpha+\gamma)\sinh(\alpha-\gamma)\} + (\alpha-\gamma)[\alpha^4A_3\sinh(\alpha+\gamma) + \gamma(\alpha+\gamma)]\left(\frac{1}{4}\alpha^2A_4\sinh(2\alpha) + \alpha\left[\left(\frac{1}{3}A_2 + A_1\right)\alpha^2 + 2A_2\right]\right)\cosh(\alpha) - \{[(A_1+A_2)\alpha^2 + 2A_2]\sinh(\alpha) + \frac{1}{2}\alpha^3A_4\}\}]} \tag{28}$$

The exact expression for the Nusselt number is obtained as:

$$Nu_w = -\frac{2}{3}\frac{(6\gamma\alpha^5 - 6\gamma^3\alpha^3)}{\kappa}\cosh(\alpha)\left(1 - \frac{\tanh(\alpha)}{\alpha}\right) \times \{-\alpha^4A_3(\alpha+\gamma)\sinh(\alpha-\gamma) + (\alpha-\gamma)[\alpha^4A_3\sinh(\alpha+\gamma) + \gamma(\alpha+\gamma)\left(\frac{1}{4}\alpha^2A_4\sinh(2\alpha) + \alpha\left[\left(\frac{1}{3}A_2 + A_1\right)\alpha^2 + 2A_2\right]\right)\cosh(\alpha) - \{[(A_1+A_2)\alpha^2 + 2A_2]\sinh(\alpha) + \frac{1}{2}\alpha^3A_4\}\}]\}^{-1} \tag{29}$$

In the limit of α going to infinity, Eq. (29) yields:

$$\lim_{\alpha\to\infty} Nu_w = 12 \tag{30}$$

This aligns well with the established value for Darcy flow [4]. At the other extreme, when the shape factor approaches zero, the behaviour resembles that of a clear fluid flow in a channel, also known as Poiseuille flow. In the limit as α tends toward zero,

$$\lim_{\alpha\to 0} Nu_w = \frac{140}{17} \tag{31}$$

This is consistent with the Nusselt number for Poiseuille flow as reported in [12].

III. RESULTS AND DISCUSSION

A. Temperature Profiles for Brinkman Extended Darcy Velocity Model

Figure 2 illustrates the effects of the heat source ratio, Q. As internal heat generation within the solid becomes more dominant relative to the wall heat flux; reflected by an increasing Q; the temperature difference between the fluid and solid phases becomes more pronounced. With higher values of Q, more heat is convected from the fluid phase, resulting in enhanced heat exchange between the solid and fluid. The figure further shows that as Q increases, a greater amount of heat is transferred from the solid to the fluid via interfacial heat exchange. Since the Biot number (Bi) is fixed, an increase in interfacial heat exchange necessitates a larger temperature difference between the two phases. This behaviour indicates that under conditions of significant internal heat generation, the local thermal equilibrium (LTE) assumption is no longer valid, and a two-equation (non-equilibrium) model becomes necessary.

It is important to note that when the temperature gradients of the fluid and solid walls are of opposite signs, the solid wall temperature gradient must be negative due to the dominating effect of heat generation in solid. This relationship can be expressed mathematically as:

$$\theta_s'(1) < 0 \tag{32}$$

By substituting the expression for the wall temperature gradient and rearranging, the critical heat source condition for the fluid and solid wall temperature gradients to have opposite signs can be expressed as:

$$\begin{aligned} Q > Q_{cr} = \tanh(\alpha)\{&Bi^2\alpha + \alpha^3\kappa^2\gamma\tanh(\gamma) \\ &-Bi\alpha^3\kappa + 2Bi^2\alpha\kappa - Bi\alpha^3\kappa^2 + Bi^2\alpha\kappa^2 \\ &-\tanh(\alpha)\,[2Bi^2\kappa + Bi^2\kappa^2 + Bi^2]\}.\{Bi\alpha^2\kappa \\ &+Bi\alpha^2\kappa^2 + 2Bi^2\kappa + Bi^2\kappa^2 - 2Bi^2\kappa - Bi^2\kappa^2 \\ &+\gamma\tanh(\gamma)\,[-\kappa^2\alpha^3\coth(\alpha) - \kappa^3\alpha^3\coth(\alpha) \\ &+\kappa^3\alpha^2 - \kappa^2Bi - \kappa^3Bi + \kappa^2\alpha Bi\coth(\alpha) \\ &+\kappa^3\alpha Bi\coth(\alpha)]\}^{-1} \end{aligned} \tag{33}$$

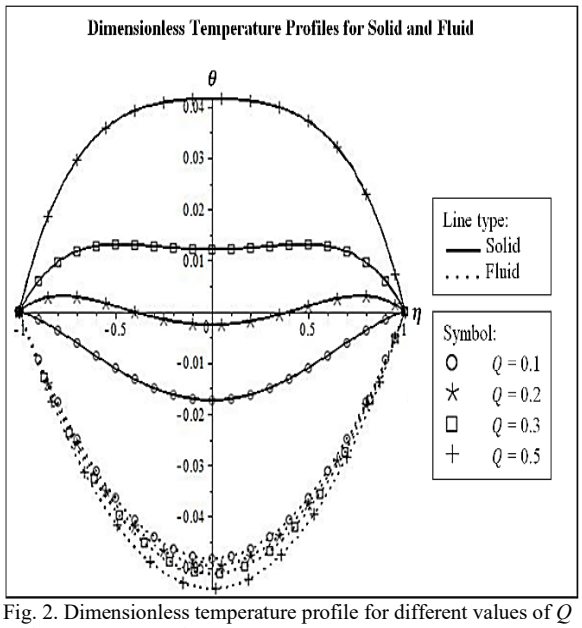

Fig. 2. Dimensionless temperature profile for different values of Q with α=0.1, κ=10 and Bi=5.

To better illustrate the heat transfer mechanism, Fig. 3 depicts the distribution of wall heat flux. Heat is convected into the fluid via two parallel pathways. In the first path, a portion of the wall heat flux is directly conducted into the fluid at the wall-fluid interface. In the second path, the remaining heat is conducted into the solid at the wall-solid interface, traverses through the solid, and is then transferred to the fluid via interfacial heat exchange.

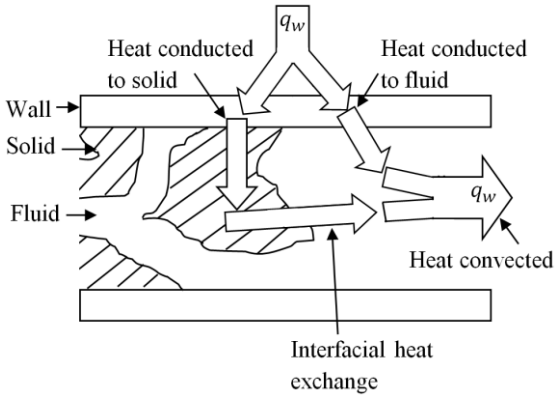

Fig. 3. Heat transfer mechanism for the boundary heat flux.

Additionally, for heat generated internally within the solid, two possible flow paths exist, depending on the value of the heat source ratio,Q. When Q is relatively small, all the internally generated heat is conducted through the solid and transferred into the fluid via interfacial exchange. However, if Q exceeds a critical threshold (as defined in Eq. 33), part of the heat generated in the solid is conducted back into the wall through the solid-wall interface and then transferred to the fluid through the wall-fluid interface, as shown in Fig. 4.

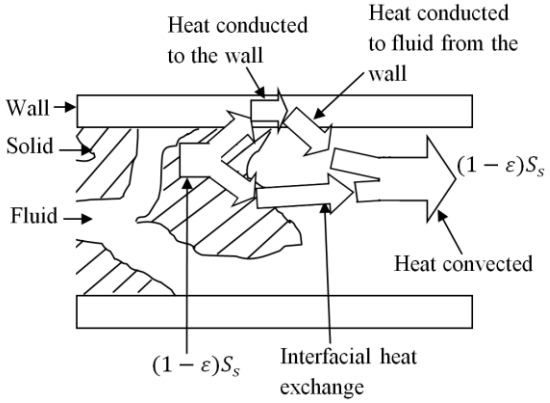

Fig. 4. Heat transfer mechanism for the heat generated in solid when Q_{cr} is exceeded.

This reversal in heat flow direction results in opposite signs for the temperature gradients of the fluid and solid at the wall. It also implies that when these gradients are dissimilar, wall heat flux is being delivered to the fluid directly through the wall-fluid interface. Regardless of the source or path, it is important to note that all heat is ultimately convected away by the fluid flow.

Figure 5 presents the variation of the critical heat generation parameter, Q_{cr}, with the thermal

conductivity ratio, κ, for three different Biot numbers. Notably, Q_{cr} decreases sharply with increasing κ, while it increases with higher Bi values. A lower κ indicates greater thermal resistance in the fluid relative to the solid, whereas a larger Biot number reflects more efficient interfacial heat exchange between the solid and fluid phases. When interfacial heat exchange is enhanced, a greater portion of the heat generated within the solid can be transferred into the fluid through the solid-fluid interface.

The shape factor of the porous medium, α, also influences Q_{cr}, albeit to a lesser extent. A larger α results in a smaller Q_{cr}, implying that a mismatch in the signs of the fluid and solid wall temperature gradients is more likely in porous media with lower permeability.

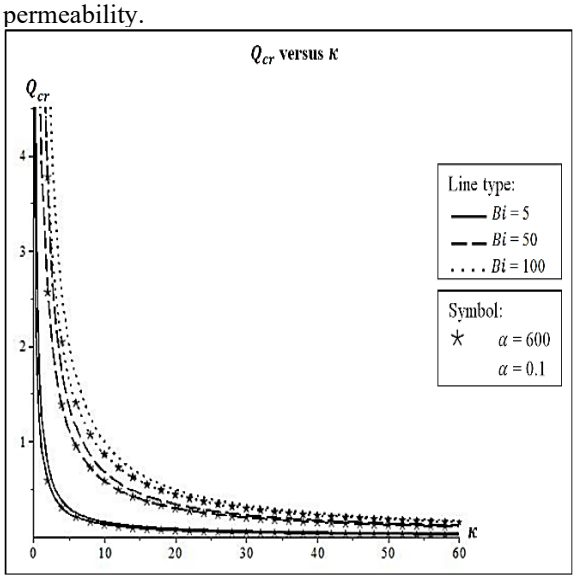

Fig. 5. A plot of Q_{cr} againts κ for various Bi and α.

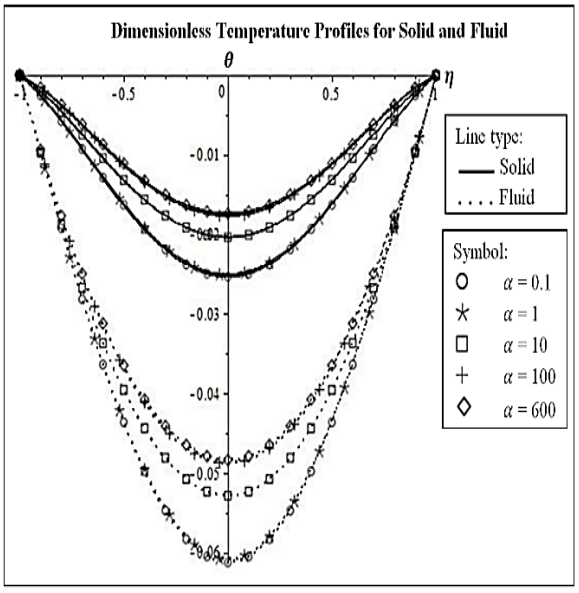

Fig. 6. Temperature profile for different α with $Q = 0.1, \kappa = 10$ and $Bi = 5$.

Figure 6 illustrates the temperature profiles for different values of α under a high κ. The profiles show only minor variation across the specified range of α, yet they are bounded by two asymptotic cases: for large α, the flow approaches Darcy behaviour; whereas for small α, the flow resembles classical Poiseuille flow in a clear fluid. The selected values of α represent these two limiting flow regimes.

B. Comparison Between 1D Temperature Profiles of Darcy (D) and Brinkman Extended Darcy (B) Velocity Model

The dimensionless temperature profiles obtained using the classical Darcy velocity model [20] and the Brinkman-extended Darcy model are compared in Fig. 7, 8, and 9. The Darcy-based temperature profiles were previously analyzed by Yang and Vafai [20]. In all comparisons, the porous medium shape factor α is fixed at 0.1 to highlight the distinctions between the two models.

Figure 7 illustrates the influence of internal heat generation Q on the temperature profiles. At low Q, both models yield similar results. However, as Q increases, the Darcy model (represented by lines with crosses) predicts a sign reversal in the temperature gradients of the solid and fluid at the wall. In contrast, this phenomenon is not observed in the Brinkman-extended Darcy model (lines with asterisks), indicating its improved capacity to account for wall effects.

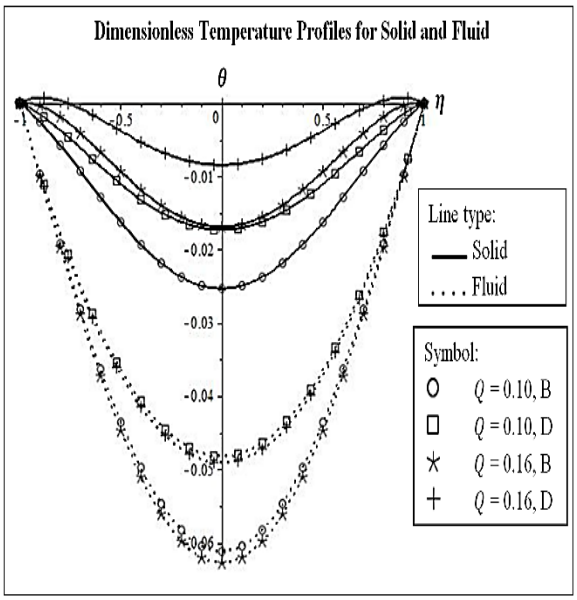

Fig. 7. Temperature profile for different Q with $\alpha = 0.1, \kappa = 10$ and $Bi = 5$.

In Fig. 8, the impact of the thermal conductivity ratio κ is examined. As κ increases, the differences between the temperature profiles predicted by the two models diminish. When κ is low, the Darcy model predicts a steeper fluid temperature gradient near the wall and a more rapid decrease in temperature towards the channel centerline, resulting in a less negative dimensionless fluid temperature at the centre. This behaviour is attributed to the uniform velocity profile assumed in the Darcy model, which enhances heat removal near the wall. However, as κ increases, the temperature gradients near the wall converge,

reflecting reduced conduction resistance in the fluid and more consistent thermal behaviour between models.

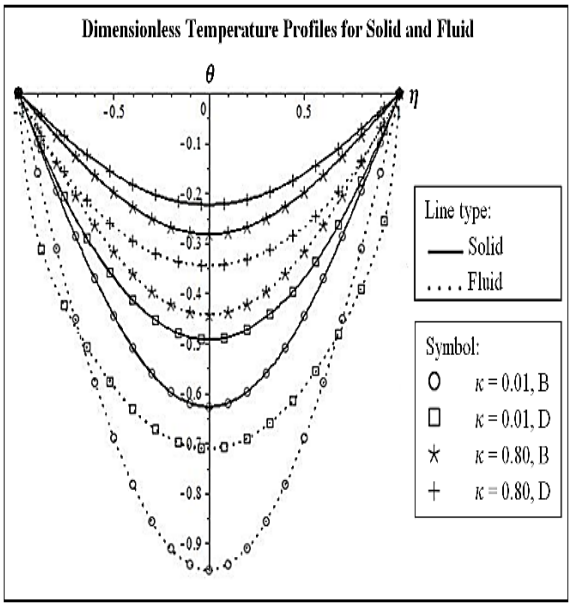

Fig. 8. Temperature profile for different κ with $Q = 0.1, \alpha = 0.1$ and $Bi = 5$.

Figure 9 presents the effect of the Biot number *Bi*. As *Bi* increases, heat transfer to the fluid improves for both models. Nevertheless, the Brinkman-extended Darcy model predicts a lower convective heat transfer rate at the wall, due to its more accurate representation of the velocity boundary layer and viscous effects near solid boundaries.

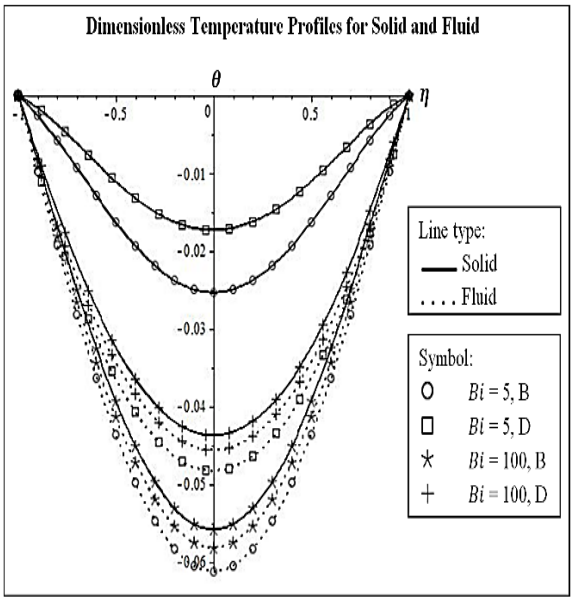

Fig. 9. Temperature profile for different Bi with $Q = 0.1, \alpha = 0.1$ and $\kappa = 10$.

C. *Two-Dimensional (2D) Temperature Profiles*

By integrating Eq. (8) [28], the two-dimensional temperature field of the fluid can be obtained. The resulting 2D temperature equation is

$$< \mathrm{T}_{2D} >^{f} (x, y) = \varphi x + < T >^{f} (y) \quad (34)$$

, where:

$$\varphi = \frac{1}{\rho_f c_{pf} < u_f >_m} \left(\frac{q_w}{H} + (1 - \varepsilon) S_s \right) \quad (35)$$

$$< T >^{f} (y) = \frac{\theta_f q_w H}{k_{s,eff}} + T_w \quad (36)$$

Differentiating Eq. (4) with respect to x yields:

$$\frac{\partial < T >^{f}}{\partial x} = \frac{\partial < T >^{s}}{\partial x} \quad (37)$$

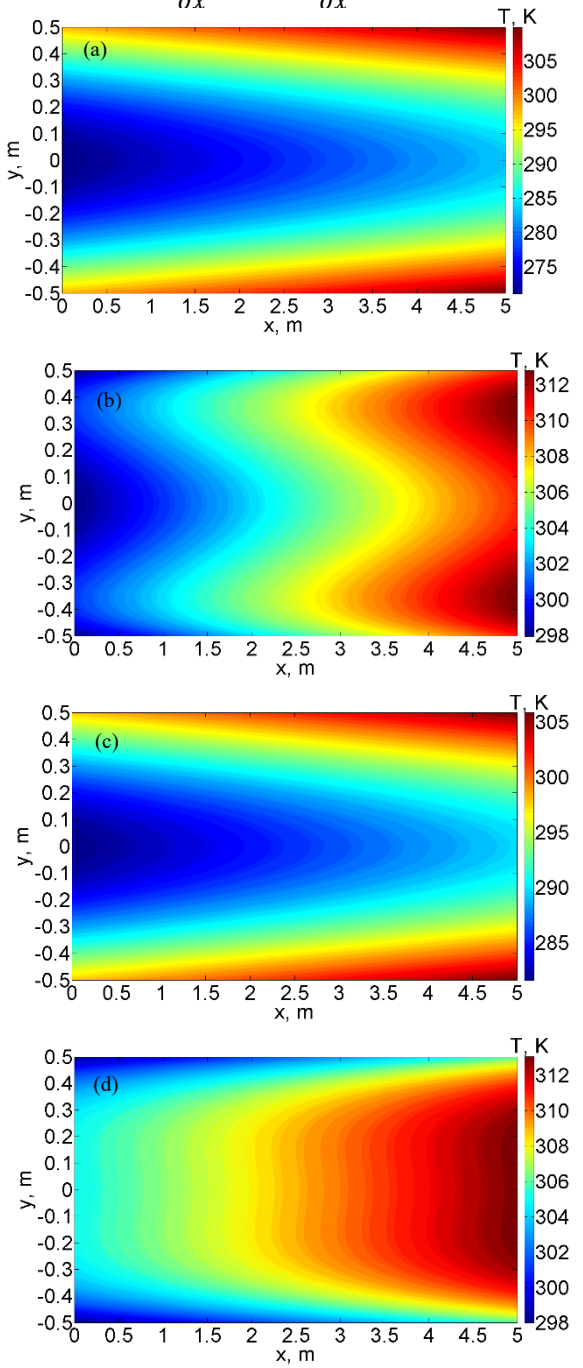

Fig. 10. 2D solid temperature profile with (a) $Bi = 5, Q = 0.28, \alpha = 0.1$ and $\kappa = 10$, (b) $Bi = 5, Q = 0.28, \alpha = 0.1$ and $\kappa = 10$, (c) $Bi = 5, Q = 0.5, \alpha = 0.1$ and $\kappa = 10$, (d) $Bi = 5, Q = 0.5, \alpha = 0.1$ and $\kappa = 10$.

Thus, the two-dimensional temperature equation for the solid phase can be expressed as:

$$< \mathrm{T}_{2D} >^{s} (x, y) = \varphi x + < T >^{s} (y) \quad (38)$$

, where:

$$< T >^{s} (y) = \frac{\theta_s q_w H}{k_{s,eff}} + T_w \quad (39)$$

The plots of Eqs. (34) and (38) for two sets of Q are shown in Fig. 10a to 10d. As illustrated in Figures 10a and 10c, the fluid temperature profiles maintain a parabolic shape across different Q values, showing minimal variation. However, the solid temperature profiles (Fig. 10b and 10d) display significantly different behaviours. This phenomenon is in agreement with Fig. 5, when Q exceeds Q_{cr}, there is an opposite solid temperature gradient at the wall, hence a varied temperature pattern in the solid.

For smaller values of Q; yet large enough to induce a sign reversal between the fluid and solid wall temperature gradients; two symmetric high-temperature cores emerge, each positioned between the impermeable wall and the channel centerline. In contrast, when Q is larger, these two cores merge, resulting in a flattened temperature distribution. Notably, in both scenarios, the peak temperature does not occur at the wall.

The influence of the porous medium shape factor, α, on the temperature profiles at the wall is evident across Fig. 10a to 10d.

D. Comparison of Nusselt Number

Figures 11, 12, and 13 illustrate the variation of Nu_w with respect to $\kappa, Bi,$ and $\alpha,$ respectively, with Q serving as the varying parameter. Across all figures, a consistent trend is observed: Nu_w predicted by the Darcy (D) model is consistently higher than that predicted by the Brinkman (B) model.

Figure 11 shows that for all values of Q, Nu_w decreases as κ increases, and approaches infinity as κ tends toward zero. Since the Nusselt number represents the ratio of convective to conductive heat transfer at the wall, a sharp increase in Nu_w occurs when the effective thermal conductivity of the fluid becomes very small. Referring back to Fig. 8 in Section 3.2, it is evident that κ dominates the behaviour of heat flux at low values, thereby strongly influencing Nu_w. Furthermore, for small Bi and for all values of κ, the overprediction of Nu_w by the D model is especially pronounced for small α when Q is low; however, the discrepancy diminishes as Q increases.

In Fig. 12, Nu_w increases with Bi, indicating a strong influence of Bi on the fluid temperature. As shown in Fig. 9, increasing Bi results in a decrease in the magnitude of the dimensionless fluid temperature, thereby increasing Nu_w. It is observed that as Q increases, Bi plays a more critical role in the discrepancy between the Nu_w values predicted by the two velocity models. For small Bi, the discrepancy tends to zero, but beyond a certain critical Bi value, a turning point emerges where the maximum difference in Nu_w occurs. This phenomenon arises because a larger Q delays the Nu_w predicted by the D model from reaching its asymptotic value, leading to maximum discrepancy at an intermediate Q.

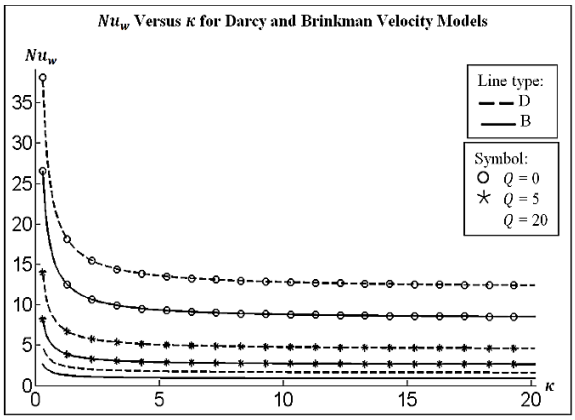

Fig. 11. Nu_w variation with κ plot for Darcy and Brinkman velocity models with $Bi = 5, \alpha = 0.1$ and various Q.

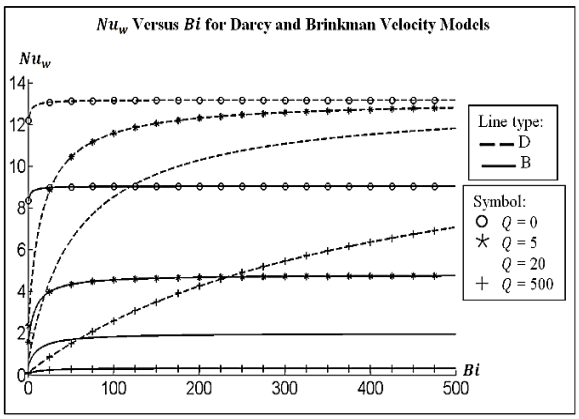

Fig. 12. Nu_w variation with Bi plot for Darcy and Brinkman velocity models with $\kappa = 10, \alpha = 0.1$ and various Q.

Figure 13 plots Nu_w versus α for the B model, with the corresponding values from the D model also included. As α approaches infinity, the Nu_w predicted by the B model converges to that of the D model, suggesting that the D model's prediction serves as an upper bound. Additionally, for the relatively small Bi value considered, the discrepancy in Nu_w between the two models vanishes as Q increases.

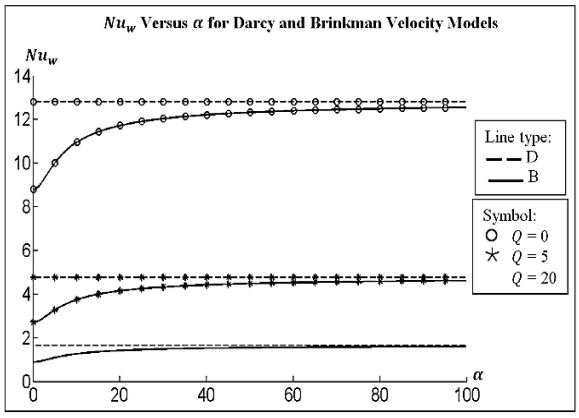

Fig. 13. Nu_w variation with α plot for Darcy and Brinkman velocity models with $\kappa = 10, Bi = 5$ and various Q.

In conclusion, for porous media with high permeability, significant discrepancies in Nu_w exist between the two velocity models when Q is small and Bi is low, regardless of κ. In contrast, at large Bi, the maximum discrepancy in Nu_w occurs at an intermediate Q value.

IV. CONCLUSION

This study presents exact solutions for forced convection in a rectangular porous channel with internal solid heat generation. Further, a critical expression for Q was derived to determine the condition under which the signs of fluid and solid wall temperature gradients differ. It was observed that in systems with relatively small shape factor α; where wall effects are more pronounced; the critical value Qcr is higher. This underscores the importance of accounting for wall effects when evaluating heat transfer characteristics in porous media.

Two velocity models; Darcy and Brinkman (extended Darcy) were compared to investigate the influence of bounding surface effects on heat transfer. While the temperature profiles and Nusselt numbers exhibit similar trends with respect to the variation of key parameters Q, κ, and Bi for both models, the Brinkman model consistently predicts lower values. As the shape factor α increases, the predictions of the Brinkman model converge to those of the Darcy model, indicating that neglecting boundary effects can lead to an overestimation of heat transfer, particularly in low-permeability porous media.

Nomenclature

a_{fs}	Specific interfacial area (m^{-1})
A_1	Function of γ, A_2, A_3 and A_4 as defined in Eq. (22)
A_2	Function of κ, Q and α as defined in Eq. (23)
A_3	Function of κ, Q, α, Bi and γ as defined in Eq. (24)
A_4	Function of κ, Q, α and Bi as defined in Eq. (25)
Bi	Equivalent Biot number as defined in Eq. (14)
c	Specific heat capacity ($J\ kg^{-1}\ K^{-1}$)
D	Hydraulic diameter (m)
Da	Darcy number, defined as $Da = K/H^2$
h_{fs}	Interfacial heat transfer coefficient ($W\ m^{-2}\ K^{-1}$)
h_w	Convection heat transfer coefficient at the wall in contact with porous medium ($W\ m^{-2}\ K^{-1}$)
H	Linear dimension of porous medium (m)
k	Thermal conductivity ($W\ m^{-1}\ K^{-1}$)
K	Permeability (m^2)
M	Viscosity ratio is defined as, $M = \frac{\mu_{eff}}{\mu}$.
Nu_w	Wall Nusselt number as defined in Eq. (26)
P	Pressure (Pa)
q_w	Constant wall heat flux ($W\ m^{-2}$)
Q	Heat source ratio as defined in Eq. (14)
Q_{cr}	Critical value of Q defined in Eq. (33)
S	Internal heat generation per unit volume ($W\ m^{-3}$)
T	Temperature (K)
u	Dimensionless fluid velocity, defined as $\frac{\mu<u_f>}{-\frac{d<P>^f}{dx}H^2}$
$< u_f >$	Extrinsic fluid velocity in longitudinal direction ($m\ s^{-1}$)
α	Porous Medium Shape Factor
κ	Fluid to solid effective thermal conductivity ratio
ρ	Density ($kg\ m^{-3}$)
η	Dimensionless y coordinates
$< \psi_i >$	Quantity averaged extrinsically, $i \in \{s, f\}$
$< \psi >^i$	Quantity averaged intrinsically, $i \in \{s, f\}$

ACKNOWLEDGEMENT

The authors would like to gratefully acknowledge the support and resources provided by Multimedia University throughout the duration of the project.

FUNDING STATEMENT

The authors received no funding from any party for the research and publication of this article.

AUTHOR CONTRIBUTIONS

Lee Jun Yang: Data Curation, Formal Analysis, Investigation, Methodology, Validation, Visualization, Writing –Original Draft Preparation; Chen Gooi Mee: Conceptualization, Formal Analysis, Methodology, Resources, Supervision, Writing –Review & Editing.

CONFLICT OF INTERESTS

No conflict of interests was disclosed.

ETHICS STATEMENTS

Our publication ethics follow The Committee of Publication Ethics (COPE) guideline. https://publicationethics.org/

REFERENCES

[1] D. Y. Lee and K. Vafai, "Analytical Characterization And Conceptual Assessment of Solid and Fluid Temperature Differentials In Porous Media," *Int. J. Heat Mass Transfer*, vol. 42, no. 3, pp. 423–435, 1999.

[2] G. Hetsroni, M. Gurevich and R. Rozenblit, "Sintered Porous Medium Heat Sink for Cooling of High-Power Mini-Devices," *Int. J. Heat Fluid Flow*, vol. 27, pp. 259–266, 2006.

[3] R. Singh, A. Akbarzadeh and M. Mochizuki, "Sintered Porous Heat Sink for Cooling of High-Power Microprocessors for Server Applications," *Int. J. Heat Mass Transfer*, vol. 52, pp. 2289–2299, 2009.

[4] M. Kaviany, *Principles of Heat Transfer in Porous Media*, Springer-Verlag, New York, 1991.

[5] A. Nakayama, F. Kuwahara, M. Sugiyama and G. Xu, "A Two-Energy Equation Model for Conduction and Convection in Porous Media," *Int. J. Heat Mass Transfer*, vol. 44, pp. 4375–4379, 2001.

[6] A. Marafie and K. Vafai, "Analysis of Non-Darcian Effects on Temperature Differentials in Porous Media," *Int. J. Heat Mass Transfer*, vol. 44, pp. 4401–4411, 2001.

[7] B. Alazmi and K. Vafai, "Constant Wall Heat Flux Boundary Conditions in Porous Media under Local Thermal Non-Equilibrium Conditions," *Int. J. Heat Mass Transfer*, vol. 45, pp. 3071–3087, 2002.

[8] G. Hwang, C. Wu and C. Chao, "Investigation of Non-Darcian Forced Convection in An Asymmetrically Heated Sintered Porous Channel," *J. Heat Transfer*, vol. 117, no. 3, pp. 725–732, 1995.

[9] V. Calmidi and R. Mahajan, "Forced Convection in High Porosity Metal Foams," *J. Heat Transfer*, vol. 122, no. 3, pp. 557–565, 2000.

[10] P. X. Jiang, "Numerical Simulation of Forced Convection Heat Transfer in Porous Plate Channels using Thermal Equilibrium and Nonthermal Equilibrium Models," *Numer. Heat Transfer Part A: Appl.*, vol. 35, no. 1, pp. 99–113, 1999.

[11] A. Amiri, K. Vafai and T. Kuzay, "Effects of Boundary Conditions on Non-Darcian Heat Transfer Through Porous Media and Experimental Comparisons," *Numer. Heat Transfer Part A: Appl.*, vol. 27, no. 6, pp. 651–664, 1995.

[12] A. Nakayama, H. Koyama and F. Kuwahara, "An Analysis on Forced Convection in A Channel Filled with A Brinkman-Darcy Porous Medium: Exact and Approximate Solutions," *Wärme- und Stoffübertragung*, vol. 23, pp. 291–295, 1988.

[13] K. Vafai and C. L. Tien, "Boundary and Inertia Effects On Flow and Heat Transfer in Porous Media," *Int. J. Heat Mass Transfer*, vol. 24, pp. 195–203, 1981.

[14] D. Poulikakos and K. Renken, "Forced Convection in A Channel Filled with Porous Medium, Including The Effects of Flow Inertia, Variable Porosity and Brinkman Friction," *J. Heat Transfer*, vol. 109, pp. 880–888, 1987.

[15] A. Dybss and R. V. Edwards, "A New Look at Porous Media Fluid Mechanics – Darcy to Turbulent," *Fundamentals of Transport Phenomena in Porous Media*, The Hague: Martinus Nijhoff, pp. 199–254, 1984.

[16] M. Kaviany, "Laminar Flow Through A Porous Channel Bounded by Isothermal Parallel Plates," *Int. J. Heat Mass Transfer*, vol. 28, pp. 851–858, 1985.

[17] K. Vafai and S. J. Kim, "On The Limitation of The Brinkman–Forchheimer–Extended Darcy Equation," *Int. J. Heat Fluid Flow*, vol. 16, pp. 11–15, 1995.

[18] K. Hooman, "A Perturbation Solution for Forced Convection in A Porous-Saturated Duct," *J. Comput. Appl. Math.*, vol. 211, pp. 57–66, 2008.

[19] S. J. Kim and D. Kim, "Forced Convection in Microstructures for Electronic Equipment Cooling," *J. Heat Transfer*, vol. 121, pp. 639–645, 1999.

[20] K. Yang and K. Vafai, "Analysis of Temperature Gradient Bifurcation in Porous Media – An Exact Solution," *Int. J. Heat Mass Transfer*, vol. 53, pp. 4316–4325, 2010.

[21] C. Yang, K. Ando and A. Nakayama, "A Local Thermal Non-Equilibrium Analysis of Fully Developed Forced Convection Flow in A Tube Filled with A Porous Medium," *Transp. Porous Media*, vol. 89, pp. 237–249, 2011.

[22] G. M. Chen, M. F. Baig, B. K. Lim and C. P. Tso, "Thermal Viscous Dissipative Couette–Poiseuille Flow in A Porous Medium Saturated Channel," *Symmetry*, vol. 11, no. 7, Art. no. 869, 2019.

[23] G. M. Chen, M. F. Baig and C. P. Tso, "Local Thermal Nonequilibrium Viscous Dissipative Couette Flow in A Porous Medium," *Spec. Topic. & Rev. in Porous Media: An Int. J.*, vol. 12, no. 6, pp. 31-41, 2021.

[24] M. U. Uwaezuoke and S. O. Ihekuna, "Heat Transfer in Couette–Poiseuille Flow Through Porous Medium," *Int. J. Res. Sci. Innov.*, vol. 11, no. 8, pp. 1313–1323, 2024.

[25] Y. M. Hung and C. P. Tso, "Effects of Viscous Dissipation on Fully Developed Forced Convection in Porous Media," *Int. Commun. Heat Mass Transfer*, vol. 36, pp. 597–603, 2009.

[26] A. Amiri and K. Vafai, "Analysis of Dispersion Effects and Non-Thermal Equilibrium, Non-Darcian, Variable Porosity Incompressible Flow Through Porous Media," *Int. J. Heat Mass Transfer*, vol. 37, no. 6, pp. 939–954, 1994.

[27] T. L. Bergman, A. S. Lavine, F. P. Incropera and D. P. DeWitt, "Internal Flow, Fully Developed Conditions," *Introduction to Heat Transfer*, 6th Edn., John Wiley & Sons, New York, pp. 497–499, 2012.

[28] T. W. Ting, Y. M. Hung and N. Guo, "Field-synergy Analysis of Viscous Dissipative Nanofluid Flow in Microchannels," *Int. J. Heat and Mass Transf.*, vol. 73, pp. 483-491, 2014.